

Seven-frequency VLBI observations of the GHz-Peaked-Spectrum source OQ 208

Wen-Feng Luo^{1,3}, Jun Yang^{2,3}, Lang Cui^{1,3}, Xiang Liu¹ ^{*} and Zhi-Qiang Shen^{2,4}

¹ National Astronomical Observatories/Urumsqi Observatory, Urumsqi 830011, China

² Shanghai Astronomical Observatory, Chinese Academy of Sciences, Shanghai 200030, China

³ Graduate University of the Chinese Academy of Sciences, Beijing 100049, China

⁴ Joint Institute for Galaxy and Cosmology, SHAO and USTC, China

Received month day; accepted month day

Abstract We present images of quasi-simultaneous VLBI observations of the GHz-Peaked-Spectrum radio source OQ 208 with the Very Long Baseline Array at 1.4, 1.7, 2.3, 5.0, 8.4, 15.4 GHz and the European VLBI Network at 6.7 GHz. The low frequency (1.4, 1.7 and 2.3 GHz) observations reveal a weak and extended steep-spectrum component at about 30 mas away in the position angle of -110° which may be a remnant emission. The radio structure of OQ 208 consists of two mini-lobes at 5.0, 6.7, 8.4 and 15.4 GHz. Our spectral analysis further confirms that the southwest lobe undergoes free-free absorption and finds that the free-free absorption is stronger in the inner region. By fitting the 8.4 GHz images from 1994 to 2005, we obtain a separation speed of 0.031 ± 0.006 mas yr⁻¹ between the two mini-lobes. This indicates a jet proper motion of 0.105 ± 0.020 c and a kinematic age of 219 ± 42 yr for the radio source.

Key words: galaxies: individual (OQ 208) – radio continuum: galaxies

1 INTRODUCTION

GHz-peaked-spectrum (GPS) sources, a sub-class of powerful radio sources ($L_{\text{radio}} \approx 10^{45}$ erg s⁻¹), lie in the Narrow Line Region with characteristics of a steep rising spectrum at low frequencies. Synchrotron self-absorption (SSA) or free-free absorption (FFA) has been proposed for the inverted spectra (O’Dea 1998). Both mechanisms are supported by some observations (e.g. Yang et al. 2005). The previous VLBI observations indicate that most of GPS galaxies exhibit either a compact double (CD) or a compact symmetric object (CSO) morphology (e.g. Stanghellini et al. 2001).

The radio source OQ 208 (B1404+286, J1407+2827; J2000.0: 14h7m0.394 + 28d27’14.69”), is one of the closest ($z = 0.077$) GPS sources with a spectral peak at 4.9 GHz (Dallacasa et al.

^{*} E-mail: liux@ms.xjb.ac.cn

2000). It is not resolved with the Very Large Array (VLA). VLBI observations (Fey et al. 1996; Stanghellini et al. 1997) revealed double mini-lobes separated by ~ 7 mas in NE-SW direction. Based on the multi-epoch VLBA observations at 2.3/8.4 GHz, Stanghellini et al. (1997, 2000) identified OQ 208 as a CSO, and determined a separation speed of 0.033 ± 0.013 mas yr $^{-1}$ between the two lobes and a kinematic age of 204 ± 81 yr.

The host galaxy of OQ 208 has a brighter core ($m_r=14.6$) and broad recombination lines and is classified as a Seyfert 1 galaxy (de Grijp et al. 1992) or broad line radio galaxy (Marziani et al. 1993). The optical image displays a low-brightness tail in the north direction toward east and indicates the presence of companions in the galactic envelope (Stanghellini et al. 1993). The X-ray observation (Guainazzi et al. 2004) discovered that OQ 208 is a Compton-thick active galactic nucleus (AGN).

The compactness of OQ 208 and its proximity to us make it a good candidate for the studies of absorption mechanisms, proper motions of jet components, and how this class of sources develops with high-resolution VLBI observation.

In this paper, we present results of the quasi-simultaneous VLBI observations at seven frequencies (1.4, 1.7, 2.3, 5.0, 6.7, 8.4 and 15.4 GHz). A new weak component at ~ 30 mas in the position angle of -110° is detected and the multi-frequency radio images and components' spectra have been obtained. The proper motion between the two mini-lobes is estimated based on our and previous 8.4 GHz VLBI data. We adopt the cosmological model with $H_0 = 70$ km s $^{-1}$ Mpc $^{-1}$, $\Omega_m = 0.3$, $\Omega_\Lambda = 0.7$ and define $S_\nu \propto \nu^\alpha$ throughout the paper.

2 OBSERVATIONS AND DATA REDUCTION

Table 1 lists some basic information of the VLBI observations. In the VLBI observations, the radio source OQ 208 was used as a fringe finder. Our VLBI observations (BY0020) were carried out at 1.7, 2.3/8.4, 5.0 and 15.4 GHz with the Very Long Baseline Array (VLBA) on May 3, 2005. OQ 208 was observed for 4 scans at 1.7 and 5.0 GHz, 6 scans at 2.3/8.4 and 15.4 GHz. Each scan lasts 4 minutes. Such repeated snap-shot mode of multiple-scans gives a good uv-coverage. The observations were made using left circular polarization, four 8-MHz channels and 2 bit sampling. The data were correlated at Socorro with 2-second integration time, 16 channels and uniform weight.

The data at 1.4 and 6.7 GHz are analyzed in order to obtain the better spectral coverage. The 1.4-GHz data are provided by Wrobel who observed OQ 208 with an 11-minute scan and 256 Mbps recording rate with the VLBA. The 6.7-GHz data are from the EVN data archive

Table 1 The related parameters of the observations and the images in Fig. 1. Col. (1), serial number of the panels. Col. (2), observation frequency in GHz. Col. (3), observation date. Col. (4), array name. Col. (5), recording rate in Mbps. Col. (6), program ID. Col. (7), peak flux density in mJy/beam. Col. (8), the lowest contour level (3σ) in mJy/beam. Col.(9-11), size and position angle of the restoring beam in mas and degree.

	Freq. (GHz)	Date	Array	Rate Mbps	Program ID	S_{peak} (mJy/b)	L.C. (mJy/b)	Maj. (mas)	Min. (mas)	P.A. ($^\circ$)
a	1.438	May 1, 2005	VLBA	256	BW0080	714.7	1.3	16.10	5.66	8.09
b	1.667	May 3, 2005	VLBA	128	BY0020	926.6	2.1	8.24	4.42	5.94
c	2.270	May 3, 2005	VLBA	128	BY0020	1290.1	1.0	9.81	8.94	42.30
d	2.270	May 3, 2005	VLBA	128	BY0020	1147.4	3.6	5.19	3.48	-3.06
e	4.987	May 3, 2005	VLBA	128	BY0020	1524.9	3.8	2.53	1.33	-1.30
f	6.668	Nov. 11, 2004	EVN	256	EN003B	978.1	11.7	5.88	0.67	77.80
g	8.420	May 3, 2005	VLBA	128	BY0020	985.7	3.2	1.31	0.96	1.18
h	15.365	May 3, 2005	VLBA	128	BY0020	346.3	2.0	0.80	0.54	0.75

(PI: Bartkiewicz). The EVN array consists of 9 stations (Cm, Jb, Ef, Mc, On, Tr, Nt, Hh and Wb). In this observation, OQ 208 was observed for 13 minutes.

The *a-priori* calibrations were done with the NRAO Astronomical Imaging Processing Software (AIPS) package (Cotton 1995). At each frequency, the amplitude calibration was performed using the system temperature measurements and antenna gain and the phase solutions were derived using the global fringe fitting with a 2-minute solution interval and a point-source model. After checking the solutions, we applied the solutions to the data, averaged all the channels in each IF and split the multi-source data into the single source data.

The self-calibration and imaging process were performed using the DIFMAP package (Shepherd et al. 1994). The overall amplitude self-calibration was not performed until the clean models had the amplitude close or equal to that of the short-baseline visibility. The gain correction for each antenna is a small factor (within 1 ± 0.15). We also fitted the calibrated visibility data to the Gaussian models using the MODELFIT program. The approximate errors of the integrated flux density and position are calculated using the formula given by Lobanov¹. The model-fitting results are reported in Table 2.

3 RESULTS

3.1 Radio morphology

The final images are displayed in Fig. 1. In each image, the lowest contour level is three times the off-source rms noise level. The contour levels increase by a factor of 2. All the images are restored using the uniform weight. The restoring beam is shown as an ellipse in the lower-left corner. The peak flux density, the lowest contour level, the size, and the position angle of the restoring beam are listed in Table 1. The model-fitting parameters of the marked components are listed in Table 2.

Our 1.4-GHz image reveals a new component marked ‘G’ in Fig. 1a, which is a weak and extended component located at ~ 30 mas and the position angle $\sim -110^\circ$. Component G also appears in the 1.7-GHz image Fig. 1b. It is resolved at 2.3 GHz in Fig. 1d when we use the full visibility data. However, it can be restored in Fig. 1c when we use the short-baseline (< 20 M λ) data. The consistence of the position of component G at the three frequencies completely confirms the existence of component G.

At the higher (> 2.3 GHz) frequencies, we do not detect component G after trying the different short-baseline data and different weighting methods. It indicates that component G is intrinsically weak. The weakness is also consistent with the extrapolation from the decreasing spectrum between 1.7 and 2.3 GHz. The radio structure of OQ 208 consists of two mini-lobes (NE and SW) at 2.3 and 6.7 GHz. The NE lobe can be fitted with three components (A, B and C) and the SW lobe with two components (E and F) at 5.0, 8.4 and 15 GHz. The 5.0 and 8.4 GHz images are consistent with the previous observations (e.g. Stanghellini et al. 1997; Fey et al. 1996). Kellermann et al. (1998, observed in 1995) found that there is a weak emission region including the core between the two lobes at 15 GHz. Comparing with their 15 GHz images, we did not detect any weak (> 1 mJy/beam) structure at 8.4 and 15.4 GHz between the two lobes although we have tried different weighting methods and (u, v) taper. It is too weak and most likely that the central core region was in a relatively quiescent period at the epoch of our observations. From the VLBA 2cm survey², we see that the emission from the central region is truly detected with the observations on Apr. 7, Dec. 15, 1995, Apr. 22, May 16, Oct. 27, 1996, Aug. 28, 1997 and Mar. 7, 1998. But from the observations on Oct. 30, 1998 to Apr. 28, 2006, nearly nothing is found in the central region. This further confirms our results at 15.4 GHz.

¹ <http://www.radionet-eu.org/wikiattach/SchoolOrganisationPages/attachments/lobanov.pdf>

² <http://www.cv.nrao.edu/2cmsurvey/>

Fig. 1 The intensity images of OQ 208 from high-resolution VLBI observations at 1.4, 1.7, 2.3, 5.0, 6.7, 8.4 and 15.4 GHz. The lowest contour level is three times the off-source r.m.s noise level. The contour levels increase by a factor of 2. The restoring beam is shown as an ellipse in the lower-left corner. The image parameters are listed in Table 1. The fitting parameters of the marked Gaussian components are listed in Table 2.

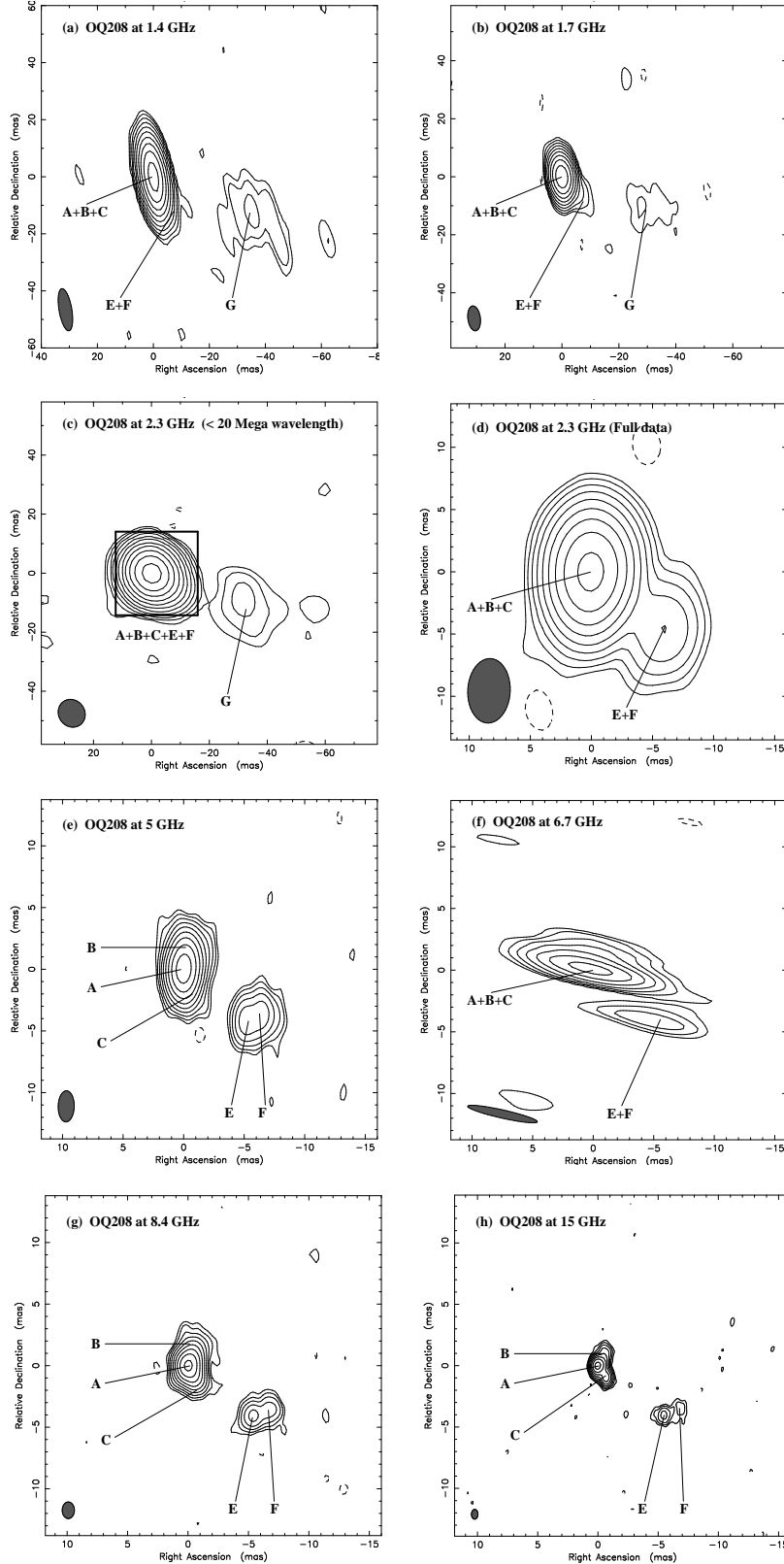


Table 2 The Gaussian components fitted with MODELFIT in the Difmap package. Col. (1), component's name. Col. (2), flux density of each component in mJy. Col. (3-4), distance and position angle with respect to component A (or A+B+C at low frequencies). Col. (5-7), major and minor axes and position angle (P. A.) of component.

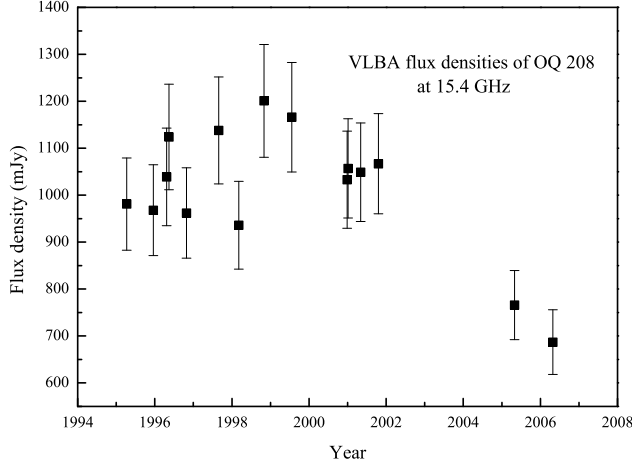
Component	Flux (mJy)	Relative Position		Size of Gaussian component		
		Radius (mas)	Θ ($^{\circ}$)	Major (mas)	Minor (mas)	P. A. ($^{\circ}$)
$\nu = 1.438$ GHz						
A+B+C	777.2 ± 67.8	0.00	—	1.98	1.39	-74.05
E+F	9.1 ± 3.0	8.24 ± 0.21	-134.19 ± 1.46	< 1	< 1	—
G	23.6 ± 8.0	39.38 ± 2.25	-109.70 ± 3.27	19.36	19.36	—
$\nu = 1.667$ GHz						
A+B+C	1010.3 ± 90.0	0.00	—	2.20	1.64	0.33
E+F	11.4 ± 4.0	8.89 ± 0.12	-129.67 ± 0.80	2.35	2.35	—
G	24.5 ± 10.5	32.10 ± 1.83	-107.63 ± 3.27	13.70	13.70	—
$\nu = 2.270$ GHz						
A+B+C	1346.1 ± 124.4	0.00	—	2.08	1.56	-8.65
E+F	66.0 ± 13.9	7.39 ± 0.37	-126.85 ± 2.87	0.79	0.79	—
G	11.5 ± 3.2	33.32 ± 4.79	-106.64 ± 8.19	11.40	11.40	—
$\nu = 4.987$ GHz						
A	1320.0 ± 122.6	0.00	—	0.74	0.48	-57.68
B	551.9 ± 62.9	1.08 ± 0.09	-21.28 ± 4.97	1.36	0.94	17.90
C	258.8 ± 35.0	1.22 ± 0.11	-167.18 ± 5.14	0.73	0.73	—
E	95.2 ± 17.4	6.63 ± 0.15	-128.91 ± 1.28	0.24	0.24	—
F	116.9 ± 21.4	7.50 ± 0.17	-119.49 ± 1.26	0.65	0.65	—
$\nu = 6.668$ GHz						
A+B+C	1979.7 ± 206.2	0.00	—	1.44	0.60	-3.46
E+F	139.7 ± 34.8	6.78 ± 0.50	-129.20 ± 4.19	1.34	0.35	-72.47
$\nu = 8.420$ GHz						
A	1046.9 ± 97.4	0.00	—	0.68	0.31	-49.07
B	317.4 ± 45.5	0.92 ± 0.10	-26.76 ± 5.95	1.32	0.89	-14.40
C	280.9 ± 35.4	1.00 ± 0.05	-146.91 ± 3.09	0.60	0.33	8.45
E	84.9 ± 17.1	6.78 ± 0.11	-127.04 ± 0.88	0.61	0.53	-5.36
F	57.7 ± 15.5	7.69 ± 0.17	-117.68 ± 1.25	0.85	0.80	-85.70
$\nu = 15.366$ GHz						
A	546.3 ± 56.4	0.00	—	0.57	0.40	-52.80
B	39.7 ± 8.1	1.27 ± 0.07	-29.28 ± 3.12	0.69	0.37	33.08
C	124.4 ± 17.3	1.18 ± 0.04	-145.63 ± 1.82	0.33	0.24	9.96
E	38.3 ± 10.5	6.79 ± 0.11	-126.76 ± 0.93	0.58	0.48	-79.03
F	16.7 ± 6.9	7.64 ± 0.22	-117.49 ± 1.62	0.92	0.61	-27.37

The integrated flux densities of the two lobes, component G and the whole source at each frequency are summarized in Table 3, and their errors are within 10% of their corresponding data. From the literature (Stanghellini et al. 1997, 2005) and our data, we can see the total flux densities of OQ 208 at 1.4 and 1.7 GHz are stable from 1980. Our VLBI flux density of OQ 208 at 2.3 GHz is 86% of the result observed with the telescope RATAN 600 at the same frequency (Stanghellini et al. 1998), indicating a small decrease.

At 5.0 GHz, the total flux density of OQ 208 observed with VLA by Dallacasa et al. (2000) decreased by about 10% compared with the data given by Stanghellini et al. (1998). Comparing with the VLBI observation by Stanghellini et al. (1997), our flux density of the NE lobe decreased by 9%, while the SW lobe is stable. We note that the total flux densities of

Table 3 The flux densities of OQ 208 in the multi-frequency VLBI observations.

Freq. (GHz)	1.438	1.667	2.270	4.987	6.668	8.420	15.365
Total (mJy)	809.9 \pm 72.6	1046.2 \pm 95.5	1423.6 \pm 130.7	2342.8 \pm 205.9	2119.4 \pm 217.4	1787.8 \pm 159.9	765.4 \pm 73.6
NE (mJy)	777.2 \pm 67.8	1010.3 \pm 90.0	1346.1 \pm 124.4	2130.7 \pm 189.0	1979.7 \pm 206.2	1645.2 \pm 148.2	710.4 \pm 68.9
SW (mJy)	9.1 \pm 3.0	11.4 \pm 4.0	66.0 \pm 13.9	212.1 \pm 30.1	139.7 \pm 34.8	142.6 \pm 24.4	55.0 \pm 14.8
G (mJy)	23.6 \pm 8.0	24.5 \pm 10.5	11.5 \pm 3.2	---	---	---	---

**Fig. 2** The VLBA total flux densities of OQ 208 at 15.4 GHz. Data are from the VLBA 2cm survey with 10% errors added, and the data on the epoch of 2005.33 is ours.

OQ 208 observed with VLA are stable within 5% from Stanghellini et al. (1998) to Tinti et al. (2005) at 8.4 GHz. The same is to the NE and SW lobes when we compare the VLBI data of Fey et al. (1996) with ours.

The total flux density of OQ 208 observed with VLA at 15.4 GHz is 1302 mJy (Dallacasa et al. 2000) and 1139 mJy (observed in 2002, Tinti et al. 2005). We have plotted the VLBA total flux densities of OQ 208 at 15.4 GHz from the VLBA 2cm survey in Fig. 2. From the figure, we find that its VLBA flux density is decreasing from the epoch 1999.55. This may result from the fading of the core since that time as we noted. Moreover, we find the flux density of the NE lobe decreased by 37% (reprocessed by us) from May 5, 2001 to Apr. 28, 2006, while the SW lobe shows stable. This also accounts for the drop of the VLBA total flux density of OQ 208 at 15.4 GHz.

We think that the core of OQ 208 was flaring in 1995-1996, or even more earlier, and gradually fading out afterwards. The fading of the NE lobe at 15.4 GHz is likely due to less energy supply from the relatively quiescent central engine in recent years. With this explanation, drop of the flux densities of OQ 208 at lower frequencies should be expected to occur with some time delay.

3.2 Proper motion

We also estimated the separation of components A and E using the available 8.4 GHz VLBI measurements over a period of about 130 months. Data for epochs 1994.52, 1997.08, 1997.25,

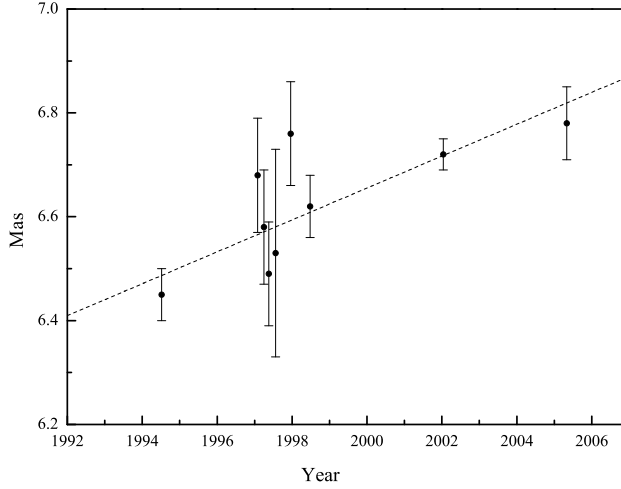


Fig. 3 Separation between components A and E in OQ 208 at 8.4 GHz.

1997.38, 1997.56, 1997.96, 1998.48, 2002.04 and 2005.33 are from Liu et al. (2000), Wang et al. (2003), the radio reference frame image database (RRFID)³ and this paper. The estimate of the position errors is obtained by using the standard deviation between the positions found by the different tasks, e.g. the tasks IMFIT, OMFIT, JMFIT and SLIME in AIPS, and MODELFIT in DIFMAP for the same components except ours that is discussed in section 2. Typical values for the position errors are between 0.03 and 0.2 mas, depending on the amount of uv-data. We plot the separation between components A and E as a function of the observing epoch in Fig. 3, and perform a linear fit to these data to estimate the separation rate between them, which is $0.031 \pm 0.006 \text{ mas yr}^{-1}$. This proper motion has confirmed the previous estimate of $0.033 \pm 0.013 \text{ mas yr}^{-1}$ by Stanghellini et al. (2000) with longer timescale data. The redshift of OQ 208 locates the source at a distance of $\sim 350 \text{ Mpc}$, at which an angular size of 1 mas corresponds to a linear size of about 1.46 pc. Then we obtain a projected jet speed of $0.074 \pm 0.014 c$. Assuming an inclination of 45° between the jet and the line of sight (Stanghellini et al. 1997), we get the actual jet velocity of $0.105 \pm 0.020 c$ and obtain a kinematic age of $219 \pm 42 \text{ yr}$ for the radio source.

We also used the data from the VLBA 2cm survey on April 7, 1995 and ours at 15.4 GHz to estimate the separation of components A and E. The result is $0.028 \pm 0.012 \text{ mas yr}^{-1}$. Both results at 8.4 and 15.4 GHz indicate that OQ 208 is expanding indeed.

4 DISCUSSION

4.1 Property of Component G

In the images at 1.4, 1.7 and 2.3 GHz (Fig. 1), component ‘G’ is far from the major components. It is difficult to explain the component G in the scenario of CSO. Component G could be a remnant emission from a previous radio burst, and OQ 208 may be a recurrent radio source. The steep spectral index ($\alpha = -2.4$) between 1.7 and 2.3 GHz further supports the remnant explanation for its emission losses (Marecki et al. 2003). Assuming a similar proper motion in

³ <http://rorf.usno.navy.mil/rrfid.shtml>

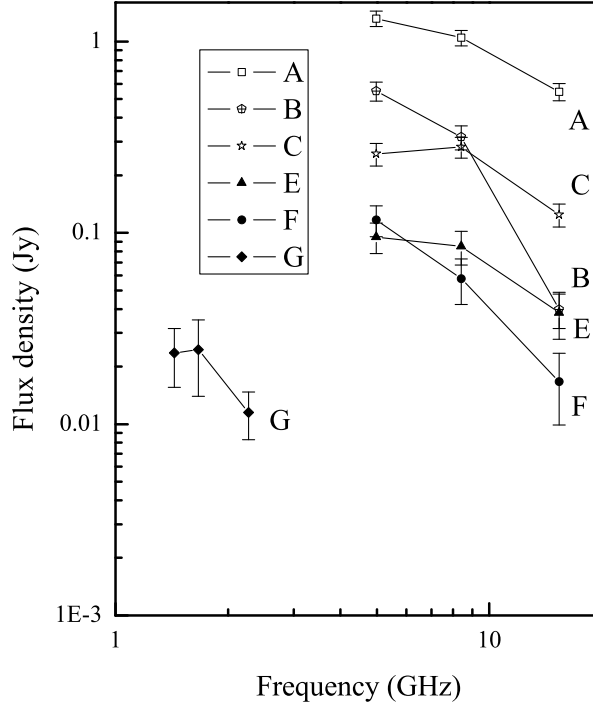


Fig. 4 Spectra of components A, B, C, E, F and G in OQ208.

the recurrent scenario, we could estimate that the age of component G is at least 1000 yr, which is much older than the CSO's age of ~ 220 yr.

With the same resolution, the flux densities of the component G are $S_{2.3\text{GHz}} = 11.5$ mJy, $S_{1.7\text{GHz}} = 24.5$ mJy and $S_{1.4\text{GHz}} = 23.6$ mJy. It has an inverted spectrum with the turnover frequency (≤ 1.7 GHz) lower than other components shown in Fig. 4. If the turnover of G component is mainly caused by SSA, then the turnover frequency in a homogenous, incoherent synchrotron radio source with a power-law electron energy distribution is given by Kellermann & Pauliny-Toth (1981)

$$\nu_t \approx 8B^{1/5}S_t^{2/5}\theta^{-4/5}(1+z)^{1/5} \quad \text{GHz} \quad (1)$$

where B is the magnetic field in Gauss, S_t the flux density at the peak in Jy, θ the angular size in mas and z the redshift. If we take $\nu_t = 1.7$ GHz, $S_t = 0.02$ Jy and $\theta = 13.7$ mas, the estimated magnetic field is $B \sim 3.5 \times 10^4$ Gauss, too large to be real. The estimate indicates that the SSA does not take effect at frequency > 1.4 GHz. Therefore, FFA could be responsible for its spectral turnover.

4.2 Absorption mechanisms

It can be estimated from Table 3 that the two lobes in OQ 208 are highly asymmetric with a flux density ratio between the north-east (NE) lobe and south-west (SW) lobe of 85 ± 21 and 89 ± 23 at 1.4–1.7 GHz, much larger than the ratios of 20 ± 2 , 10 ± 1 , 14 ± 2 , 12 ± 1 and 13 ± 2

at frequencies 2.3, 5.0, 6.7, 8.4 and 15.4 GHz, respectively. The asymmetric free-free absorption has been used to interpret the large flux density ratio between NE and SW lobes (Kamenno et al. 2000). Considering the radio photons from the receding lobe is more scattered than that from the approaching lobe in the line of sight, Thomson scattering was also introduced to the flux density ratio of OQ 208, but it only contributes a factor of 1.7 for the ratio (Liu et al. 2003). Xie et al. (2005) introduced the Doppler effect into the fit to the observed spectra, and found that two models, i.e. the FFA+beaming model and the SSA+beaming model, can fit the spectrum of the NE lobe equally well. Our observations offer the wider spectral measurements by adding a new low frequency 1.4 GHz data, and thus can be used to test the different models. However, it is still hard to discriminate which absorption mechanism is the dominant process for the NE lobe. As for the SW lobe that has a turnover frequency ~ 4 GHz, SSA only is definitely not enough to account for a steep spectral index of $\alpha = 5.7$ between 1.7 and 2.3 GHz because the value is much larger than the maximum attainable spectral index ($\alpha = 2.5$) by the SSA model.

Fig. 4 shows the spectra of the pc-scale components of OQ 208. The inner components A, C and E have a similar spectrum. Compared with the inner components, the outer components B and F have steeper high-frequency spectra. The flux density ratio between the counter components E and F is 2.3 at 15 GHz, 1.5 at 8.4 GHz and 0.8 at 5 GHz. The decrease at 5 GHz could be further explained by the small free-free opacity difference in the SW lobe. Using the uniform FFA-opacity model (e. g. Kamenno et al. 2001), component E has a turnover frequency $\nu_t = 5.6$ GHz and component F has $\nu_t = 3.7$ GHz. Based on the projected distance of component G from the core, we can give a lower limit to the characteristic size of the external plasma, i.e. ~ 57 pc, which is larger than that of any components. Therefore, the assumption of the uniform FFA-opacity model is effective for the two components. Both the decrease of the flux ratio and the estimated turnover frequencies agree well, indicating that component E has a higher FFA opacity than component F at the same emission frequency. Furthermore, component G has the lower turnover frequency (≤ 1.7 GHz) than components E and F. Therefore, it seems that the turnover frequency decreases from the inner component E to the outer component G. This infers that the FFA is stronger in the inner region.

4.3 Free-free radiation

Free-free radiation is thermal radiation. The radiation from the source propagates through the foreground plasma, whose excitation temperature is the same as the electron temperature T_e , and attenuated. The spontaneous thermal radiation from the plasma is added. Thus, the observed brightness temperature T_b can be written as:

$$T_b = T_{b0} \exp(-\tau_f \nu^{-2.1}) + T_e [1 - \exp(-\tau_f \nu^{-2.1})] , \quad (2)$$

where T_{b0} is the intrinsic brightness temperature of radio source in K and τ_f the FFA coefficient at 1 GHz. If the source is optically thin ($\nu > \nu_t$), then $T_b \approx T_{b0}$. For OQ 208, the brightness temperature of the lobe or hot spot is $\sim 10^9$ K (e.g. Liu et al. 2002), which is much higher than the thermal temperature $T_e \sim 10^5$ K (Kamenno et al. 2001). If the source is optically thick ($\nu < \nu_t$), the second item will be close to T_e . We will expect that T_{b0} increases with the decrease of frequency and is close to the inverse Compton limit $\sim 10^{12}$ K at a certain frequency if the source has a power-law spectrum with $\alpha < 0$. If we adopt $\tau_f = 8$ (Xie et al. 2005), $\exp(-\tau) \sim 3 \times 10^{-4}$ at 1 GHz and the first item is still much larger than T_e . Therefore, for our observations at frequencies greater than 1 GHz, the free-free radiation can be omitted.

5 SUMMARY AND CONCLUSIONS

We present the results of the quasi-simultaneous VLBI observations of the GPS radio source OQ 208 at seven frequencies (1.4, 1.7, 2.3, 5.0, 6.7, 8.4 and 15.4 GHz). We detected a weak and extended component G at about 30 mas in the position angle of -110° at 1.4, 1.7 and 2.3 GHz. The component G is supposed to be a relic emission from an old radio burst and its age is estimated to be at least 1000 yr assuming a similar jet proper motion in the CSO. Though both SSA and FFA can fit the spectrum of the NE lobe well, the SW lobe must undergo FFA considering its rising spectral index of $\alpha = 5.7$ between 1.7 and 2.3 GHz, larger than 2.5 the maximum attainable spectral index for SSA. The FFA is stronger in the inner region than in the outer region.

We estimate a separation speed of 0.031 ± 0.006 mas/yr between components A and E based on the 8.4 GHz VLBI observations at 9 epochs and further estimate a kinematic age of 219 ± 42 yr for OQ 208. The proper motion (0.105 ± 0.020 c) of the lobe confirms that estimated by Stanghellini et al. (2000) with longer timescale data.

Acknowledgements We thank the referee for valuable comments and J. Wrobel for providing us the 1.4 GHz VLBA data. VLBA (Very Long Baseline Array) is a facility of the National Radio Astronomy Observatory (NRAO), operated by Associated Universities, under cooperative agreement with the National Science Foundation. We thank the MOJAVE (Lister and Homan, 2005, AJ, 130, 1418) and 2cm Survey (Kellermann et al., 2004, ApJ, 609, 539) programs. This work has made use of Radio Reference Frame Image Database of the United States Naval Observatory. The European VLBI Network is a joint facility of European, Chinese, South African and other radio astronomy institutes funded by their national research councils. Z.-Q. Shen acknowledges the support in part by the National Natural Science Foundation of China (grant 10573029), Program of Shanghai Subject Chief Scientist (06XD14024), and the One-Hundred-Talent Program of Chinese Academy of Sciences.

References

- Cotton W. D., 1995, In: J. A. Zensus, P. J. Diamond, P. J. Napier, eds., Very Long Baseline Interferometry and the VLBA. ASP Conference Series 82, 189
- de Grijp M. H. K., Keel W. C., Miley G. K., Goudfrooij P., Lub J., 1992, A&AS, 96, 389
- Dallacasa D., Stanghellini C., Centonza M., Fanti R., 2000, A&A, 887, 900
- Fey A. L., Clegg A. W., Fomalont E. B. 1996, ApJS, 105, 299
- Guainazzi M., Siemiginowska A., Rodriguez-Pascual P., Stanghellini C., 2004, A&A, 421, 461
- Kellermann K. I., Pauliny-Toth I. I. K. 1981, ARA&A, 19, 373
- Kellermann K. I., Vermeulen R. C., Zensus A. J., Cohen M. H., 1998, AJ, 115, 1295
- Kameno S., Horiuchi S., Shen Z.-Q., Inoue M., Kobayashi H., 2000, PASJ, 52, 209
- Kameno S., PhD Thesis, 2001
- Liu X., Stanghellini C., Dallacasa D., Bondi M., 2000, Chin. Phys. Lett., 17(4), 307
- Liu X., Stanghellini C., Dallacasa D., Zhang H. Y., 2002, A&A, 385, 768
- Liu X., Yang J., 2003, AcASn, Vol.44, 296, 298
- Marziani P., Sulentic J. W., Calvani M., Perez E., Moles M., Penston M. V., 1993, ApJ, 410, 56
- Marecki A., Barthel P. D., Polatidis A., Owsianik I., 2003, PASA, 20, 16
- O’Dea C. P., 1998, PASP, 110, 493
- Stanghellini C., Baum S. A., O’Dea C. P., Laurikainen E., 1993, ApJ, 88, 1
- Stanghellini C., Bondi M., Dallacasa D., O’Dea C. P., Baum S. A., Fanti R., Fanti C., 1997, A&A, 318, 376
- Stanghellini C., O’Dea C. P., Dallacasa D., Baum S. A., Fanti R., Fanti C., 1998, A&A, 131, 303

- Stanghellini C., Bondi M., Dallacasa D., Liu X., 2000, In: Conway J. E., Polatidis A. G., et al., ed., EVN 5th Symp., Goteborg: Chalmers Technical University, p. 99
- Stanghellini C., Dallacasa D., O'Dea C. P., Baum S. A., Fanti R., Fanti C., 2001, *A&A*, 377, 377
- Stanghellini C., O'Dea C. P., Dallacasa D., Cassaro P., Baum S. A., Fanti R., Fanti C., 2005, *A&A*, 891, 902
- Shepherd M. C., Pearson T. J., Taylor G. B., 1994, *BAAS*, 26, 987
- Tinti S., Dallacasa D., de Zotti G., Celotti A., Stanghellini C., 2005, *A&A*, 432, 31
- Wang W. H., Hong X. Y., An T., 2003, *ChJAA*, Vol.3, No.6, 505
- Xie G. Y., Jiang D. R., Shen Z. -Q., 2005, *ApJ*, 621, L13
- Yang J., Liu X., Shen Z. -Q. 2005, *ChJAA*, Vol.5, No.6, 563